Renewable Energy 147 (2020) 1704–1717

Contents lists available at ScienceDirect

Renewable Energy

journal homepage: www.elsevier.com/locate/renene

Numerical study on performance improvement of a flat-plate solar collector filled with porous foam

K. Anirudh, S. Dhinakaran*

The Centre for Fluid Dynamics, Discipline of Mechanical Engineering, Indian Institute of Technology Indore, Simrol, Indore, 453 552, India

ARTICLE INFO

Article history:
Received 1 April 2019
Received in revised form
15 August 2019
Accepted 12 September 2019
Available online 16 September 2019

Keywords:
Flat-plate solar collector
Porous metal foam
Buoyancy
Radiation
Rosseland model
Darcy-Brinkman-Forchheimer model

ABSTRACT

Performance improvement of a flat-plate solar collector is studied numerically using computational fluid dynamics based opensource tool, OpenFOAM. The collector channel is filled with fully saturated porous metal foam, and extended Darcy-Brinkman-Forchheimer model is used to model this porous region. The present code has been tested thoroughly against various numerical and experimental works from the literature, and a reasonable agreement is achieved. The influence of permeability (Darcy number, $Da = 10^{-4}$ - 10^{-1}), radiation insolation parameter ($Rd = 0$ - 5), buoyancy parameter (Richardson number, $Ri = 0$ - 5), and collector channel inclination angle ($\alpha = 0^{\circ}$ - 45°) on the collector channel outlet temperature i.e., effective heating achieved has been studied. The novelty of the present study lies in the implementation of Rosseland approximation for modelling radiation influence, along with buoyancy consideration by varying channel inclination angles. The computational results suggest that the flow and thermal fields vary when modelling buoyancy and radiation influences combined. The insertion of porous metal foam enhances the thermal performance because of better thermal mixing, along with buoyancy parameter and volumetric radiation parameter. Although the performance does improve with the channel inclination angle, the maximum increment is obtained at intermediate angles, while any further rise in inclination gives a minor performance improvement. A comparison of different boundary conditions along with Rosseland approximation usage is given. A remark on the inclusion of the Forchheimer term in the present flow regime is given. The manuscript provides an impetus for further experimental work on the present case and comments on buoyancy parameter influence on channel performance.

1. Introduction

Dependency on fossil fuel as a prime energy source has led to high and ever-rising energy costs and limitation in its supply. Concerns about climate change become serious every day, as the environmental and health-related issues of the burning of fossil fuels rise, as more fuels are consumed to meet the energy demands. Already, discussions on ecological changes have aggravated due to the heatwave, breakdown of ocean conveyor belt circulation and collapse of major ice sheets due to global warming. Also, more recently, the advent of heat islands seems to increase due to the rising population in megacities, which demands a higher cooling load. The urban cooling load may sometimes increase up to 25% when compared to surrounding rural areas to cope up with warming [1].

In the future, the population of earth will rise, which compels us to look for a cleaner energy option, keeping the present environmental scenario into perspective. Solar energy, the most abundant of all conventional energy sources, has been considered to be a promising option for coping up with the present and future energy demands. Solar thermal systems are one of the most exciting technologies that interest engineers. Flat plate solar collectors (FPSC) are the oldest solar thermal system, which is also most applied. FPSCs are nothing but heat exchangers which convert incident radiant solar energy into heat, very similar to the greenhouse effect. The construction consists of an insulated metal box with a glass or plastic cover and a dark coloured absorber plate. The high thermal conductivity plate absorbs incident radiation and transfers it to the circulating fluid, which is to be heated. Usually, this type of solar collectors is used in low-temperature applications due to its lower efficiency. The thermal efficiency of the FPSC can be increased by various recent optimisation methods and advanced

* Corresponding author.
E-mail address: sdhina@iiti.ac.in (S. Dhinakaran).

https://doi.org/10.1016/j.renene.2019.09.038
0960-1481/

Nomenclature

$\bar{s}$	velocity of fluid in porous region (m/s)
$\dot{Q}$	volume flow rate (lit/min)
C_p	specific heat at constant pressure $(J/kg{\cdot}K)$
d	diameter of the spherical particle of packed bed (m)
D_h	hydraulic diameter (m)
Da	Darcy number (κ/D_h^2)
F	inertial factor, $((1.75/\sqrt{150}){\cdot}(1/\varepsilon^{1.5}))$
f_D	dimensionless pressure drop (friction factor)
H	collector channel height (m)
k	thermal conductivity of the material $(W/(m{\cdot}K))$
k_{eff}	effective thermal conductivity, (k_e/k_f)
L	collector channel length (m)
Nu	local Nusselt number $(-k_{eff}(\partial\theta)/(\partial Y))$
P	dimensionless pressure $(p/(U_\infty^2))$
p	kinematic pressure of the fluid (m^2/s^2)
Pr	Prandtl number (ν/α)
Q	Radiation absorption parameter
q_w	radiative heat flux (W/m^2)
Rd	Volumetric radiation parameter $((4\sigma T_\infty^3)/(kk^*))$
Re	Reynolds number $(U_\infty{\cdot}D_h/\nu)$
Ri	Richardson number $(g\beta(T_w - T_\infty)/D_h)$
T	dimensional temperature (K)
t	dimensional time (s)
U,V	non - dimensional x -, y - component of velocity $(u/U_\infty, \nu/V_\infty)$
u,v	x -, y - component of velocity (m/s)
X,Y	non-dimensional horizontal, verical distance $(x/L, y/H)$
x,y	horizontal, vertical distance (m)

Greek

α	channel inclination angle (°)
Δ	largest grid size (m)
δ	smallest grid size (m)
ε	porosity
κ	permeability of the material (m^2)
ν	kinematic viscosity (m^2/s)
ρ	density (kg/m^3)
τ	non-dimensional time $(t{\cdot}U_\infty/D_h)$
θ	non-dimensional temperature $((T - T_\infty)/(T_w - T_\infty))$

Subscript

∞	far field value
eff	effective value
in	inlet value
m	mean value
w	value at the top absorber wall

technology and materials. Two critical components of FPSC, the working fluid, and the absorber plate have been fine-tuned in several ways to enhance the overall performance of the collector. Porous materials can be effectively used as a passive way of improving heat transfer, and they have always attracted researchers in the past few decades. In particular, porous metal foams, are of prime importance in solar thermochemical reactors and thermal collectors. Due to the presence of voids, porous materials have been used to store thermal energy and enhance thermal performance and, to control flow instabilities like vortex shedding [2]. Furthermore, they promote fluid mixing, which in turn results in higher thermal conductivity of the fluid. Near the wall, if a porous layer is laid down, it results in a higher thermal gradient at the wall, which results in lower thermal resistance to the flow. Also, if the heat is first conducted through a material, through which the circulating fluid can pass, heat absorption should considerably increase. Hence, it would be further interesting to look for possibilities of design uplifting in solar collectors or heat exchangers with the aid of porous foam insertion [3].

Extensive literature is available on analytical, numerical and experimental approaches dealing with porous filled solar collector channels, for both single and double pass type collectors. Lansing et al. [4] obtain better heat dissipation from energy-absorbing solid using porous media and they study its use in a solar collector with air as working medium. They provide temperature distribution within a gas-cooled porous flat plate collector using analytical solutions. Their results show that improvement in thermal performance of the collector of around 102% can be obtained through porous insertion when compared to the non-porous type collectors. Sorour [5] develop a generic design for a solar collector for heating water, wherein buoyancy is the only driving force for fluid movement, without using pumps or sophisticated controls. They report an efficiency of almost 80% for achieving at the outlet temperature of lesser than 50 °C at high flow rates. Kleinstreuer and Chiang [6] suggest porous-medium flat-plate solar collector as an interesting alternative to conventional fin-and-tube designs for water heating, for cases where higher pumping power is not a major concern. From their numerical results, it is seen that porous solar collector has higher thermal efficiency in comparison to non-porous type conventional flat-plate collectors. They advocate the usage of the non-Darcy approach to accurately model the fluid flow and heat transfer dynamics inside the porous channel. Sopian et al. [7] perform experiments to study the effects of porous insertion, in the form of steel wool, on the thermal performance of a double-pass solar air collector. Improvement in the thermal efficiency of about 20–70% is obtained by inserting the porous material into the lower channel. Yousef and Adam [8,9] simulate single- and double-pass porous-filled and empty flat plate collector numerically. Authors find a deep influence of channel length, flow rate and porous medium thickness on the thermal efficiency. Double-pass configuration is found to be more efficient than single-pass, due to increased heat removal. Xu et al. [10] study forced convective heat transfer in a metal-foam filled solar collector analytically, subjected to the no-slip adiabatic condition. They look into Darcy, Brinkman, and Forchheimer models for flow and Local Thermal Equilibrium (LTE) and Local Thermal Non-Equilibrium (LTNE) assumptions for the energy equation. It is understood that as the porosity of the metal foam is increased, LTNE model significance becomes lesser in the porous medium. Further, to evaluate the thermal performance of metal foam, a combined fin-LTE model is suggested. Jouybari et al. [11] experimentally study the thermal performance of a filled porous channel FPSC with SiO_2-deionised water nanofluids. The influence of nanofluid concentration on thermal efficiency is found to more than the flow rate of the channel. Authors advocate the combined use of nanofluid with porous media for improvement in thermal performance of the solar collector. Jouybari et al. [12] further provide another experimental investigation of the thermal performance and pressure loss of a flat plate solar collector, filled with porous medium. Results suggest that at lower values of Reynolds number, the insertion of the porous medium results in increased optical efficiency and reduced heat losses. However, at higher Reynolds number, heat losses increase due to the presence of the

porous medium. Nusselt number value increases significantly in the case of porous medium filled collector when compared with the empty channel. The resulting increase in pressure drop, in turn, the pumping power is not dramatic enough to use higher capacity pumps. Saedodin et al. [13] both, numerically and experimentally study a porous medium filled FPSC by varying the porous substrate thickness and flow rate in the channel. The filled channel is reported to have the highest thermal performance. When the flow rate was increased, the dimensionless temperature gradient at the upper wall of the channel was found to increase, resulting in a lower temperature difference between the wall and fluid. Consequently, the Nusselt number augmented relatively up to 82% with porous inserts. Also, the LTE assumption was preferred over LTNE for calculating the thermal performance of the porous insert solar collector. Inserting a porous medium is seen to improve the absorbed energy parameter up to 18.5%. However, the dimensionless pressure drop is observed to increase when using the porous insertion, but the growth was not dramatic enough for a greater source of electric power.

Further, performance improvement through porous substrate placement instead of filling is studied. Al-Nimr and Alkam [14] improve tubeless conventional collector performance by introducing porous substrates at the inner side of the collector absorber plate. Authors claim that an increment in *Nu* up to 25 times can be achieved through the filling of the channel up to 50% by the porous substrate. Beyond this thickness, they did not report any significant increase in collector thermal performance. However, the pressure drop because of this insertion also incremented up to 30 times in comparison to the empty channel. The insertion of a porous layer up to an optimum thickness yields a significant rise in thermal efficiency with a moderate rise in pumping cost. Alkam and Al-Nimr [15] improve the thermal performance of a tube-type solar collector by placing the porous layer at the inner walls of tubes. An improvement in convection heat transfer is seen through the increment in Nusselt number up to 27 times due to the porous medium. The thermal efficiency follows a rise by 15–130%. However, the pressure drop also increases up to 32 times. A critical substrate thickness value of around 0.8, beyond which no significant increase in heat transfer is reported. Kareem et al. [16] provide a comparative study between conventional single-pass solar collector with a plane glass wall (glazing layer) and a double-pass collector design with gravel as a porous insertion in the lower channel of absorber plate. Authors suggest that an enormous amount of heat loss occurs at different boundaries surrounding the absorber plate for single-pass design. Double-pass design reduces heat transfer losses, and along with gravel insertion, thermal performance further increases. Rashidi et al. [17] provide sensitivity analysis on the influence of Darcy number, Reynolds number, porous substrate thickness on the combined convection-radiation heat transfer in a heat exchanger filled with a porous medium of different thickness. The sensitivity analysis reveals that Reynolds number affects pressure drop and Nusselt number lesser at high Darcy number and porous medium thickness values. Also, the Nusselt number is sensitive to the porous substrate thickness at higher thickness values. Bovand et al. [18] analyse combined convection-radiation heat transfer in a porous FPSC with varying porous layer thickness. It is seen that the Nusselt number increases with the porous layer thickness at higher values of Darcy number, while at lower Darcy number the converse is true. The average Nusselt number is reported to increase with the volumetric radiation parameter.

Few other ways of introducing porous medium are also explored in the literature. Chen and Huang [19] carry out a numerical analysis for higher heat transfer from a strip heat source, kept in a solar channel, by discrete metal-foam blocks. Insertion of metal-foam blocks at the inner wall of absorber turned out to be an effective method of improving the thermal performance of the channel. *With proper optimisation of the porous block properties, and adjusting the pressure drop accordingly, thermal efficiency also can be increased due to the presence of metal-foam block.* Hirasawa et al. [20] experimentally study the reduction of natural convection heat loss from a solar thermal collector by positioning a high-porosity porous medium above the collector plate. Authors advocate placement of porous medium above collector to curb the upward convection and conduction heat losses. An increment in the overall thermal efficiency of the thermal collector was reported. Huang et al. [21] insert four metal blocks at the inner side of the absorber wall and subject them to pulsating flow. In their numerical analysis, this method of enhancing heat transfer between the absorber and working fluid was declared to be efficient. Chen et al. [22] numerically simulate the melting process of paraffin with aluminium foams using a two-temperature model in a solar flat-plate water heater. A significant improvement in the melting rate and temperature distribution in the paraffin is found in the presence of the aluminium foam insertion. Anirudh and Dhinakaran [23] performed numerical computations to study the performance of a flat-plate solar collector inserted with porous blocks. Paramount improvement in thermal performance was reported by insertion of a single thin long porous block near the absorber wall.

From the above review, it is lucid that porous medium filled FPSCs have better thermal performance and lesser heat losses. However, to the best of Authors' knowledge, no numerical work on FPSC has considered both, *buoyancy and proper radiation model* for modelling solar insolation. In the present numerical endeavour, a detailed analysis of the influence of buoyancy term (Richardson number, *Ri*) and volumetric radiation parameter (*Rd*) is put forth. Also, hereafter, the volumetric radiation parameter is referred to as just the radiation parameter. Further, variation in thermal performance of FPSC at various inclination angles of the porous channel (α) is also given. A comment on the inclusion of the Forchheimer term in the modelling of porous metal foam is given while comparing extended Darcy-Brinkman-Forchheimer model and Darcy-Brinkman model. The numerical results presented in this manuscript shall provide an impetus for experimental efforts in the insertion of the porous layer of various porous properties along with inclination of the channel body and numerical modelling with more realistic radiation models and boundary conditions.

2. Mathematical formulation

2.1. Problem description

Numerical computations are performed for studying the laminar, incompressible and steady flow through a two-dimensional collector channel (direct absorption type), which is filled with metal-foam as shown in Fig. 1. The primary aim of the current study is to investigate the performance enhancement of the collector channel due to variation in the porous and buoyancy parameters. Also, the influence of Radiation parameter is to be studied. The fluid is assumed to be water with a Prandtl number (*Pr*) value of 7. Dimensions of FPSC are inspired by the combined numerical and experimental study by Saedodin et al. [13]. Channel length and height are set to 0.8 m and 0.013 m, respectively. The thickness and optical properties of glass and absorber plate are neglected. Both of these plates have been assumed to be a single layer, which is not abnormal and occurs quite frequently in the literature on FPSC channels [13,17,18]. The common plate is exposed to a uniform and constant wall heat flux, which mimics the solar insolation. However, this does not represent the radiation model, and the radiative heat flux is introduced in the energy equation through the Rosseland approximation. A porous metal foam, with

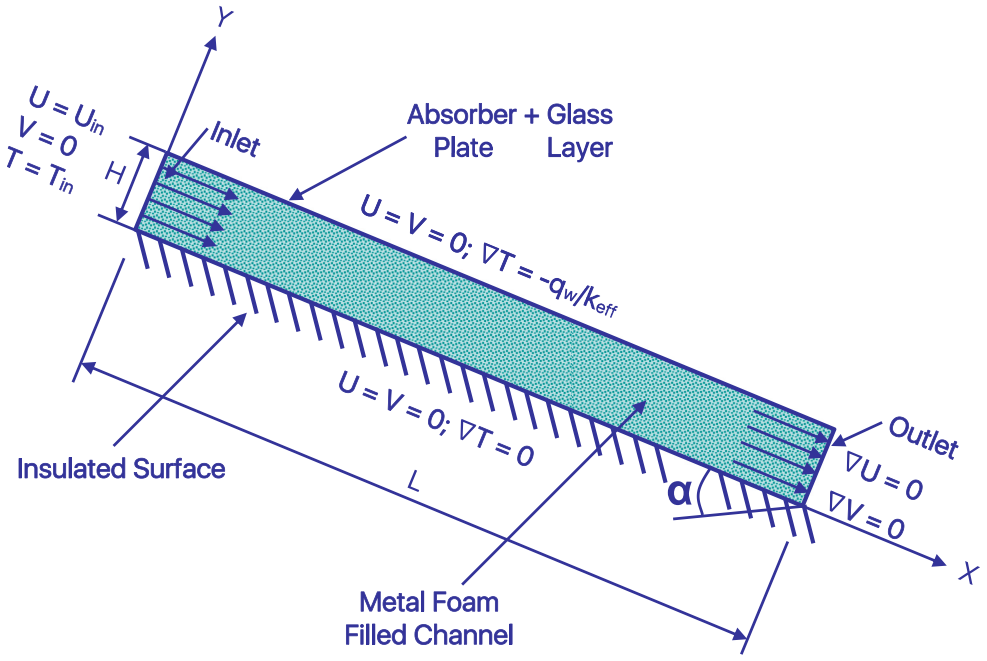

Fig. 1. Schematic of the computational setup for the flow through FPSC, along with boundary condition details, exposed to solar radiation and subjected to thermal buoyancy.

uniform porosity and permeability, is inserted into the FPSC until the entire area is occupied. The fluid (water) enters the domain with a uniform horizontal velocity distribution (U_∞) and temperature (T_∞). A constant flow rate of 0.5 lit/min, corresponding to a Reynolds number value of around 144, is considered. At the upper absorber plate, a uniform heat flux (q_w) is incident along the entire channel length, which represents the solar insolation. The channel inclination angle (α) is varied to study the combined influence of buoyancy and angle variation on the hydrodynamic and thermal performance of porous FPSC. In order to make the current problem amenable for numerical simulations, it is assumed that the porous insertion is homogeneous and isotropic and is saturated with a single-phase fluid. Fully developed flow is desired in the porous channel, while fluid and solid temperature are expected to be equal, i.e. local thermal equilibrium (LTE) condition is assumed. This condition can be safely taken in cases where slow warming exists, like the present case of warming of water.

2.2. Governing equations

Considering the assumptions as mentioned earlier, governing equations require suitable modifications to model flow, and heat transfer in the porous media filled FPSC, which is subjected to radiation insolation. Fluid flow, in the absence of the porous medium, occurs with an artificial velocity, also referred to as superficial velocity. However, the physical or actual velocity can vary with a location inside the complex porous region, and it is difficult to be calculated, while superficial velocity is relied on because it is easily known and is unambiguous. Open area for superficial flow through the pores gets lesser due to the presence of the porous medium, which in turn results in higher velocity in this region. The dimensionless entity that relates physical and superficial velocity is porosity, which is nothing but volume fraction of voids of the entire porous medium. Hence, the physical velocity is related to the superficial velocity as $\bar{s} = v/\varepsilon$, and this introduces the '1 /ε' term next to velocity terms in the transport equation [24]. Additionally, for modelling the viscous and inertial resistance to the flow, two source terms viz., Darcy and Forchheimer terms are introduced in the momentum equations, respectively. Darcy term takes into account the existence of general porous resistance in the flow, while Brinkman coefficient (advection term along with porosity) brings into the viscous resistance offered by the porous zone to the fluid flow. Forchheimer term, the second source term, looks after the inertial resistance offered by the porous media at higher *Re*. Darcy-Brinkman-Forchheimer extended model is the most applied numerical approach when it comes to flow through porous media [25–29]. However, the validity of the additional Forchheimer term is still under doubt, and for the FPSC filled with porous media for the current parameter ranges, this term has not been tested yet. A comment on the use of this inertial term is provided in this manuscript in Sec. 5.7.

It should be noted that thermophysical properties of the fluid at a reference temperature are taken to be constant, except for the buoyancy term in x - and y - momentum equations, i.e. the Boussinesq approximation is taken into consideration. A source term is introduced in the momentum equation regarding gravity, thermal expansion coefficient and the temperature difference between the hot surface and the entire numerical domain.

It is well-known that the porous foam strongly absorbs the incident radiation. Therefore, it is considered to be optically thick with a short radiation transport mean free path. The Rosseland approximation is suitable for an optically thick media and is hence used in this study [30]. It is introduced in the energy equation through a source term "$-(\partial q_{wx}/\partial x + \partial q_{wy}/\partial y)$", where q_w is the incident radiation, and it can be written as,

$$q_{wx} = -\frac{4\sigma}{3\beta_r}\frac{\partial T^4}{\partial x}, \text{and } q_{wy} = -\frac{4\sigma}{3\beta_r}\frac{\partial T^4}{\partial y} \quad (1)$$

where, σ = Stefan-Boltzmann constant and β_r = extinction

coefficient. The fluid-phase temperature differences within the flow are assumed to be sufficiently small so that T^4 can be written as a linear function of temperature by expanding it in a Taylor series about the free-stream temperature, T_∞. The higher-order terms are neglected so that the expansion burns down to $-T^4 = 4T_\infty^3 T - 3T_\infty^3$. Using this deduction along with Eqn. (5), the source terms can be introduced in the governing equations as.

Continuity Equation:

$$\frac{\partial u}{\partial x}+\frac{\partial v}{\partial y}=0, \tag{2}$$

Momentum Equations:

$$\rho\left(\frac{u}{\varepsilon^2}\frac{\partial u}{\partial x}+\frac{v}{\varepsilon^2}\frac{\partial u}{\partial y}\right)=-\frac{\partial p}{\partial x}+\frac{\mu_e}{\varepsilon}\left(\frac{\partial^2 u}{\partial x^2}+\frac{\partial^2 u}{\partial y^2}\right)-\frac{\mu}{\kappa}u-\frac{\rho F}{\sqrt{\kappa}}\left|\vec{V}\right|u - g\beta(T-T_\infty)\sin\alpha, \tag{3}$$

$$\rho\left(\frac{v}{\varepsilon^2}\frac{\partial v}{\partial x}+\frac{v}{\varepsilon^2}\frac{\partial v}{\partial y}\right)=-\frac{\partial p}{\partial y}+\frac{\mu_e}{\varepsilon}\left(\frac{\partial^2 v}{\partial x^2}+\frac{\partial^2 v}{\partial y^2}\right)-\frac{\mu}{\kappa}v-\frac{\rho F}{\sqrt{\kappa}}\left|\vec{V}\right|v - g\beta(T-T_\infty)\cos\alpha, \quad \text{and,} \tag{4}$$

Energy Equation:

$$\left(\frac{u}{\varepsilon}\frac{\partial T}{\partial x}+\frac{v}{\varepsilon}\frac{\partial T}{\partial y}\right)=\left(1+\frac{4}{3}Rd\right)\alpha\left(\frac{\partial^2 T}{\partial x^2}+\frac{\partial^2 T}{\partial y^2}\right) \tag{5}$$

In the above equations, $\left|\vec{V}\right| = \sqrt{u^2+v^2}$ is the resultant velocity, $F = \frac{1.75}{\sqrt{150}}\cdot\frac{1}{\varepsilon^{1.5}}$ is the inertial factor [25], $Rd = \frac{4\sigma T_\infty^3}{k\beta_r}$ is radiation insolation parameter.

2.3. Non-dimensionalisation of results

Using non-dimensional variables in OpenFOAM 5.0 is quite cumbersome, and hence, non-dimensionalisation of the output variables is done post-simulation, by using the following characteristic scales,

$$X=\frac{x}{L}, Y=\frac{y}{H}, P=\frac{p}{\rho U_\infty^2}, U=\frac{u}{U_\infty}, V=\frac{v}{U_\infty} \quad \text{and} \quad \theta=\frac{T-T_\infty}{T_w-T_m}. \tag{6}$$

2.4. Boundary conditions

Details of boundary conditions imposed on the computational domain are displayed in Fig. 1. At inlet of the porous FPSC, a uniform flow at an ambient temperature is introduced through $U = U_{in}$, $V = 0$, $T = T_{in}$ and $\nabla P = 0$. At outlet of the domain, the 'inletOutlet' boundary condition is used. Normally, this treatment gives a fully developed condition in terms of $(\partial U)/(\partial X) = 0$, $V = 0$, $\nabla T = 0$ and $P = 0$. In the case of any reversal in the flow direction, the horizontal velocity is automatically set to a fixed value (which is 'zero', as in real condition no backflow is expected to occur). The bottom of porous channel is insulated to avoid heat losses and a 'no-slip' boundary condition is imposed by $U = V = 0$, $\nabla P = 0$ and $\nabla T = 0$. The top wall is exposed to solar radiation heat flux 'q_w', while 'no-slip' boundary condition is imposed throughout the wall by $U = V = 0$, $\nabla P = 0$ and $\nabla T = -q_w/k_{eff}$.

3. Numerical details

For modelling flow and heat transport in a metal foam filled porous FPSC, numerical simulations are performed using the finite volume method and the open-source tool OpenFOAM [31] is used. The generic 'buoyantBoussinesqSimpleFoam' solver (based on the combination of the SIMPLE algorithm) of OpenFOAM is improvised by applying the Darcy-Forchheimer-Brinkman model and the Rosseland approximation to it. This solver is robust in handling laminar and steady problems and hence, is chosen for the present computations. The steady-state scheme is used to account for the time derivative, while Gauss linear scheme is used for the gradient, divergence (bounded type) and Laplacian terms and a linear interpolation scheme is used for the collocated grid. Further, PCG solver with DIC pre-conditioner is used for the pressure term, and PBiCG solver with DILU pre-conditioner is used for evaluating the velocity and temperature terms. Although OpenFOAM does not use an explicit Rhie-Chow correction, the generic correction for pressure terms is believed to be 'Rhie-Chow inspired' [32]. The residual criteria for pressure, velocity and temperature terms is set to 10^{-6}. An under-relaxation of 0.3, 0.7 and 0.98 are applied for pressure, velocity and temperature terms, respectively.

4. Grid generation and code validation

The generic blockMesh tool of OpenFOAM is used for the generation of structured non-uniform mesh in the computational domain, as shown in Fig. 2. A uniform mesh is used up to $0.0077H$ from the top and bottom side of the channel, followed by a non-uniform mesh up to the centre. The element size is $0.000385H$ in the uniform region, which lasts to 20 grids, beyond which the grids

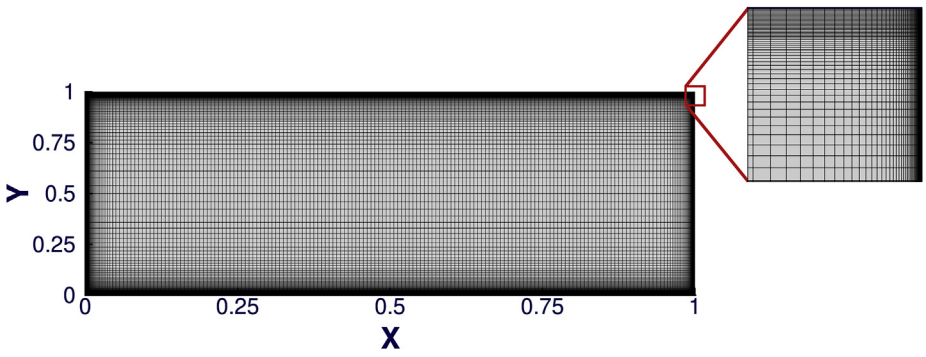

Fig. 2. Non-uniform structured distribution of mesh in the computational domain for simulating the steady incompressible fluid flow.

Table 1
Grid dependence test, for various grid sizes, on local Nusselt number (Nu) calculated at the top right corner of the collector channel and friction factor (f_D). Percentage difference is calculated with respect to finest mesh, Grid D. Symbol '*' represents chosen grid for the study. The test is carried out at $Ri = 5$, $Da = 10^{-4}$, $Rd = 5$ and $\alpha = 45^{o}$.

Grid (M x N)	Nu	Deviation (%)	f_D	Deviation (%)
A (154 × 76)	19.2830	2.218	207.0972	0.050
B (231 × 114)	19.0659	1.067	207.1548	0.022
C* (308 × 152)	18.8894	0.131	207.1832	0.008
D (385 × 190)	18.8646	0.000	207.2002	0.000

grow to a maximum size of 0.0385H in the centre of the channel. Similarly, at the left and right end of the channel, a uniform mesh is used up to 0.000125L distance, with the grid size of 0.00000625L. A non-uniform mesh spans up to a distance of 0.0625L, and it grows

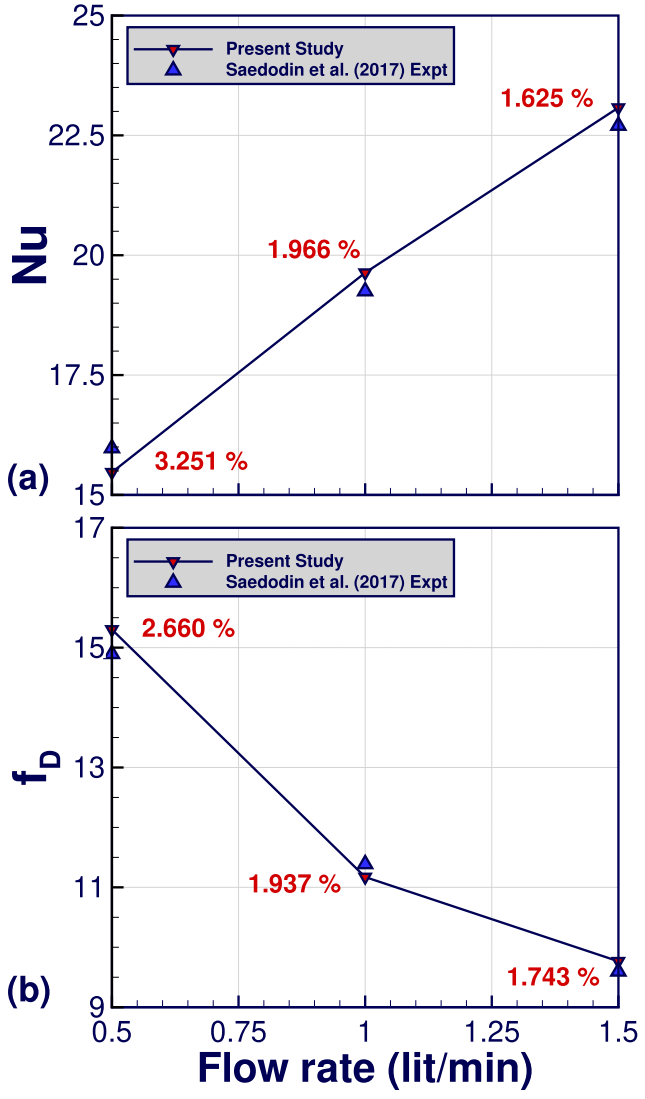

Fig. 3. Comparison of mean Nusselt number for verification of present numerical code with the computational results of (a) Basak et al. [34] at the bottom wall of the porous cavity for various values of Darcy number, Da at Rayleigh number, $Ra = 10^6$; (b) Varol et al. [33] at the cold size wall of an empty cavity with a corner heater for various values of Darcy number, Da at Rayleigh number, $Ra = 10^5$; (c) Ahmed et al. [35] at the cold size wall of a porous cavity with a corner heater for various values of Darcy number, Da and radiation parameter, Rd at Rayleigh number, $Ra = 10^5$.

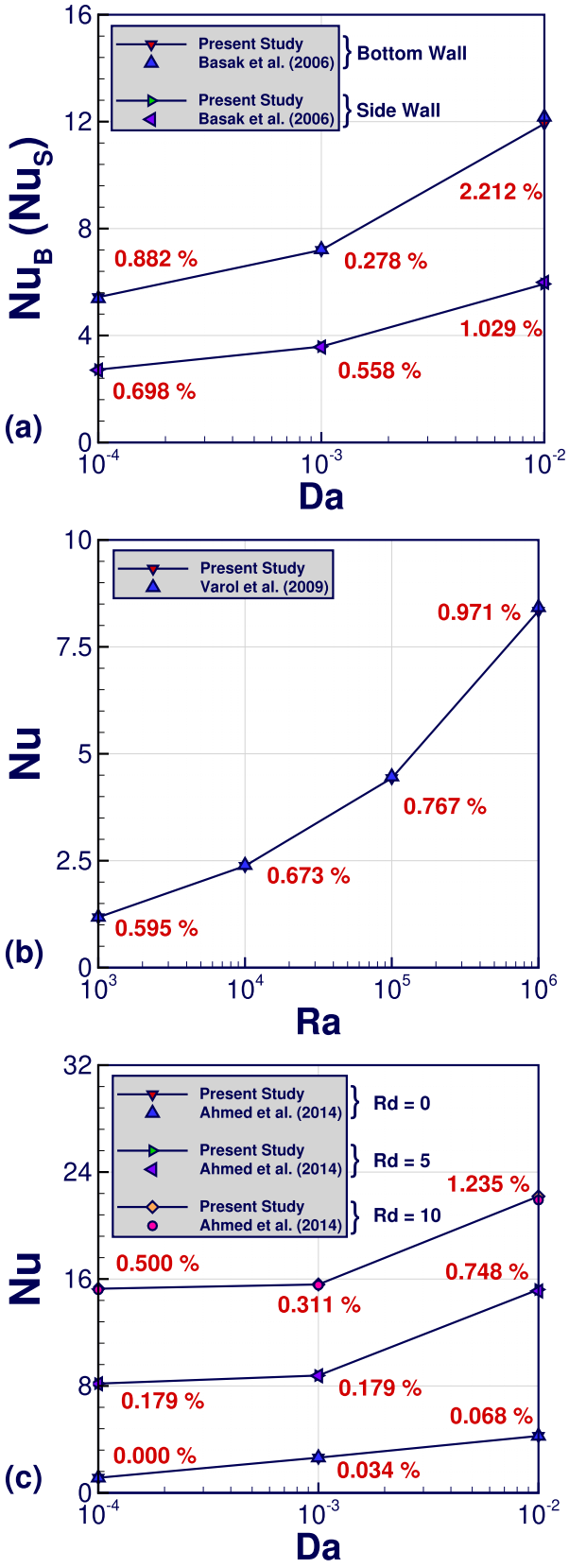

Fig. 4. Comparison of local Nusselt number at the top-right corner of FPSC outlet and friction factor across the domain with the experimental results of Saedodin et al. [13] at various flow rate values.

to 0.00625*L* grid size. For a distance of 0.875*L*, a uniform mesh is used with 0.00625*L* size. Further, a grid dependence study should be carried out at the extremities of parameter ranges to check whether the code generates results independent on the choice of grid size. The grid sensitivity analysis is performed at $Rd = 5$, $Ri = 5$ and $\alpha = 45^{\circ}$ on critical parameters related to flow (friction factor, f_D) and heat transfer (Nusselt number, *Nu*) phenomena. Several test simulations are run exploring the optimal grid size for the given FPSC dimension. Current solver is tested for four different grids of X × Y sizes viz., 154 × 76 (Grid A), 231 × 114 (Grid B), 308 × 152 (Grid C) and 385 × 190 (Grid D) (see Table 1). The test is carried out lower values of permeability, keeping in mind that at such values, the viscous and inertial resistance to flow is higher in comparison to permeability values above $Da \geq 10^{-4}$. After a close rumination of the given values, considering both accuracy and computational economy, Grid C is chosen. *The current solver is verified with the experimental results of Saedodin* et al. [13] *at various flow rates, and satisfactory confidence is obtained.* Furthermore, the present numerical recipe is tested for both simple cavity heat transfer, buoyancy and radiation model implementations with the numerical works by Varol et al. [33], Basak et al. [34] and Ahmed et al. [35], respectively. Details of the verification with the numerical works can be seen in Fig. 3, while validation with experimental data is shown in Fig. 4. Sufficient confidence is achieved in the present numerical code by this extensive verification and validation, allowing to proceed with the numerical experiments.

5. Results and discussions

Extensive two-dimensional numerical computations are carried out for understanding the influence of *Da*, *Rd*, *Ri* and α on the flow patterns and heat transfer performance of a solar flat plate collector filled with porous metal foam. Various values of permeability considered are $Da = 10^{-4}$, 10^{-3}, 10^{-2}, and 10^{-1}. The theoretical extremities of no-flow and through-flow conditions are covered through these permeability levels. In order to model the significance of buoyant forces on flow and heat transfer in the FPSC channel, various Richardson number, *Ri* values taken are 0, 1, 2, and 5. Also, the cumulative effect of buoyancy and inclination of the channel is studied by tilting the collector at 0°, 15°, 30°, and 45°, which covers a decent range to conclude.

5.1. Non-dimensional horizontal velocity and isotherm contours

When the water flows into the porous FPSC channel filled with the metal foam, after travelling a certain distance, a fully developed flow condition is established before the flow reaches the outlet of the collector. It is well-known that for higher values of Prandtl number, similar to the present case, the hydrodynamic boundary layer is thicker than the thermal boundary layer. Interaction of these boundary layers due to the influence of buoyancy and volumetric radiation is explored in the present study. Details of the horizontal velocity and temperature fields and the impact of various governing parameters on the same can be visualised through Figs. 6–8. The flow physics of empty as well as channels filled porous materials are well understood. In an empty collector, for a fully developed flow condition, the horizontal velocity profile assumes a parabolic shape at the outlet. Also, the temperature profile is more like a smooth half parabolic curve, right from the top heated to the cold bottom wall. Such kind of stature of both the fields arises due to the influence of the stationary wall. They progress from the wall surface to the centre of the channel, because fluid flows in the horizontal direction towards the outlet. The contours have been shown for $\alpha = 45^{\circ}$, $Ri = 5$, $Da = 10^{-2}$, and $Rd = 0$ in general, except while the effect of particular variable is studied. The trend more or less exists for other values as well.

As the buoyancy is considered during numerical modelling, the flow field is seen to be profoundly affected by varying channel inclination angles in Fig. 5(I) and (II). For a horizontal collector ($\alpha = 0^{\circ}$), the hydrodynamic boundary layer remains unchanged throughout the top and bottom walls, while at the outlet, it thickens abruptly, as shown in Fig. 5(I-a). Such occurrence is happening because of the vertical direction of buoyancy, which is perpendicular to the cross-flow, and such a cross-buoyancy condition expands the thermal plume near the wall, causing heat to dissipate further away from the absorber wall of the channel. As a result, a lesser thermal gradient should exist near the absorber wall, which further expands at the collector outlet, as seen in Fig. 5(II-a). As the channel inclination angle increases, the hydrodynamic boundary layer thickens along with the absorber plate and thins at the insulator. At the outlet, however, the reverse exists. The tendency of the free-falling of water increases with α, which is supported by the increasing velocity shown by darker flood contours crowding in the channel and at the outlet. A similar phenomenon exists in the temperature field, as seen through Fig. 5(II). Thermal boundary layer thickens along with the absorber plate, but towards the end of the channel, thinning is noticed.

When the channel is horizontal, and no buoyancy influence is taken into account, both the hydrodynamic and thermal boundary layers are uniform in nature and span well throughout the channel length. As the Richardson number is increased, evidently the hydrodynamic boundary layer remains unchanged throughout the absorber and insulator plates, but at the outlet, it thickens abruptly, as shown in Fig. 6(II-b). Isotherm contours too show similar trait as seen in Fig. 6(I). Perhaps the buoyant forces can be used to aid the heat exchange between the hot absorber plate and the working fluid by inclining the collector clockwise, which also supports the free movement of the fluid under gravity, assuring lesser need of pumping power. At higher channel inclination angle, $\alpha = 45^{\circ}$, the same can be witnessed in Fig. 6(II-c) and (II-d), wherein although throughout the collector length a thick thermal boundary layer exists at absorber wall, it acutely thins at the outlet. Also, a significant increase in the horizontal fluid velocity is apparent with the appearance of darker flood contours in Fig. 6(I-c) and (I-d). Therefore, a higher outlet fluid temperature is assured, due to this aiding action of the buoyancy. Also, the increment in horizontal velocity values suggests the smoother movement of fluid across the porous channel, causing a lesser need of pumping power.

At $Da = 10^{-4}$, very little flow occurs through the channel, and hence, very thin boundary layer form at the absorber wall. When the Darcy number of the porous metal foam insertion is increased between $Da = 10^{-4}$ - 10^{-1}, severe thickening of both, hydrodynamic and thermal boundary layers are witnessed, due to enhanced fluid flow throughout the channel. Again, due to buoyancy and channel inclination effect, they both thin at the outlet of the collector. This phenomenon can be visualised through Fig. 7(I) and (II). Although the considered range of Darcy number covered theoretical possibilities of no-flow and through-flow conditions, intermediate values of Darcy number give a more realistic touch to the considered range. Moreover, most of the discussion is carried out for $Da = 10^{-2}$, which more or less represents the intermediate or realistic Darcy number regime for the present porous metal foam filling the FPSC channel.

The Rosseland approximation application for collector channel has been performed for the first time. Usually, in applications of such studies [35], the heat transfer is measured at the cold sections, wherein with the radiation parameter, the rise in Nusselt number is obtained. However, for mixed convection heat transfer, with an increase in Radiation parameter, severe thickening of hydrodynamic and thermal boundary layers occurs (see Fig. 8(I) and (II)).

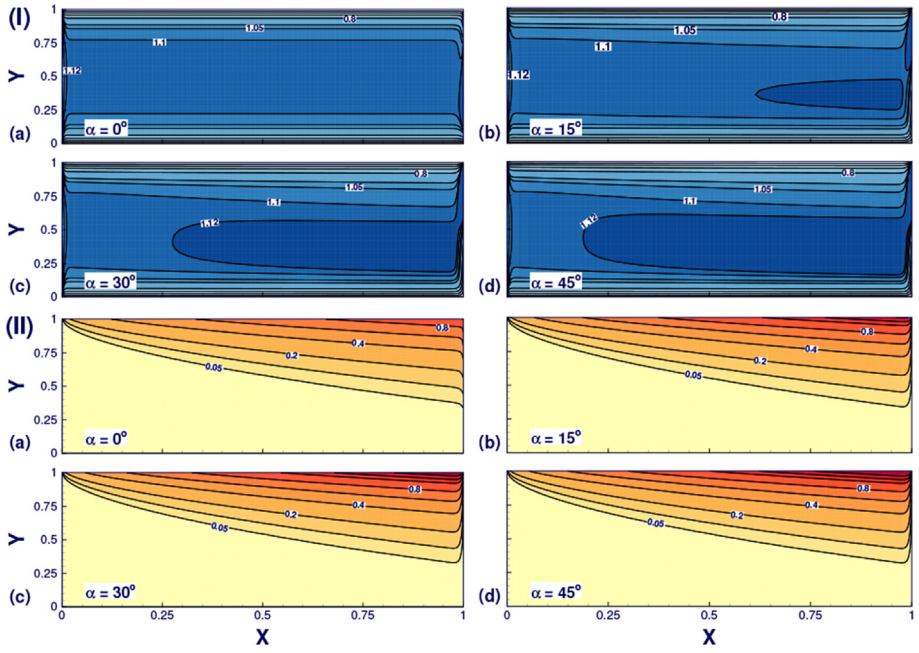

Fig. 5. (I) Velocity and (II) Isotherm contours in FPSC channel for different channel inclination angle (α) values. The contours are shown at Richardson number, $Ri = 5$, Darcy number, $Da = 10^{-2}$ and Radiation parameter, $Rd = 0$.

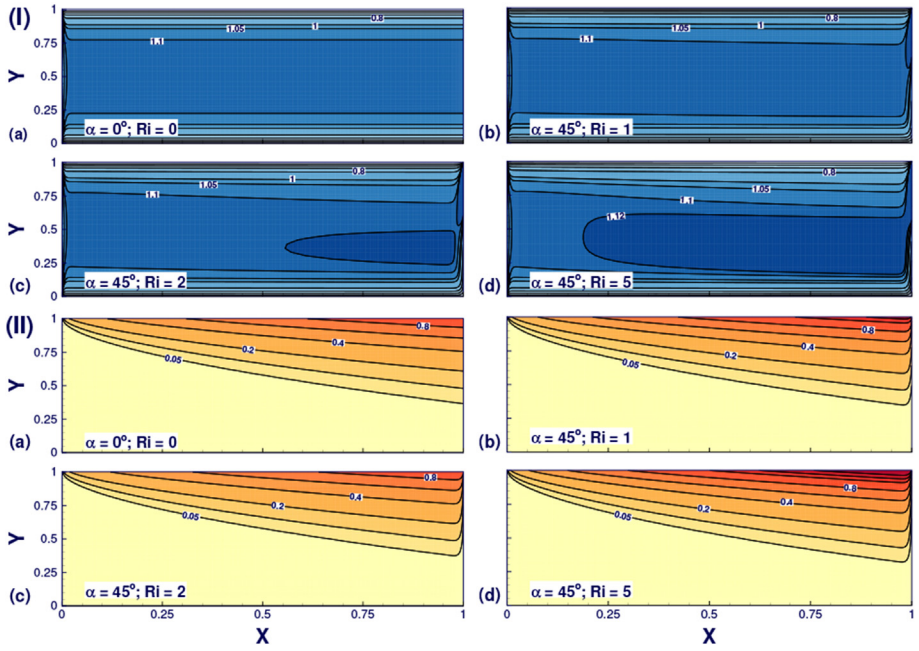

Fig. 6. (I) Velocity and (II) Isotherm contours in FPSC channel for different channel inclination angle (α) and Richardson number (Ri) values. The contours are shown at Darcy number, $Da = 10^{-2}$ and Radiation parameter, $Rd = 0$.

Although at the outlet the boundary layers again cling to the absorber plate, the intensity looks fair in comparison to lower *Rd* values. Such happenings can be ascertained to the point that Radiation parameter is being introduced as a multiple to diffusion term, wherein, the overall effect would be similar to reducing Prandtl number. It is well understood that at lower *Pr* values, the viscous diffusion rate is lesser, and hence, the increment in boundary layer thickness occurs [36]. The overall effect of this should be a reduction in the heat transfer rate. Details about the same can be seen through horizontal velocity and temperature profiles at the collector outlet given below.

5.2. Non-dimensional horizontal velocity distribution

The primary aim of an FPSC is to maximise temperature of the circulating fluid leaving the channel, i.e. most of the incident solar radiation is to be transferred to fluid flowing in the channel. As a result, the flow at the outlet of the channel is expected to be fully developed and uniformly heated to the maximum extent. For making this happen, the present channel is kept sufficiently long to

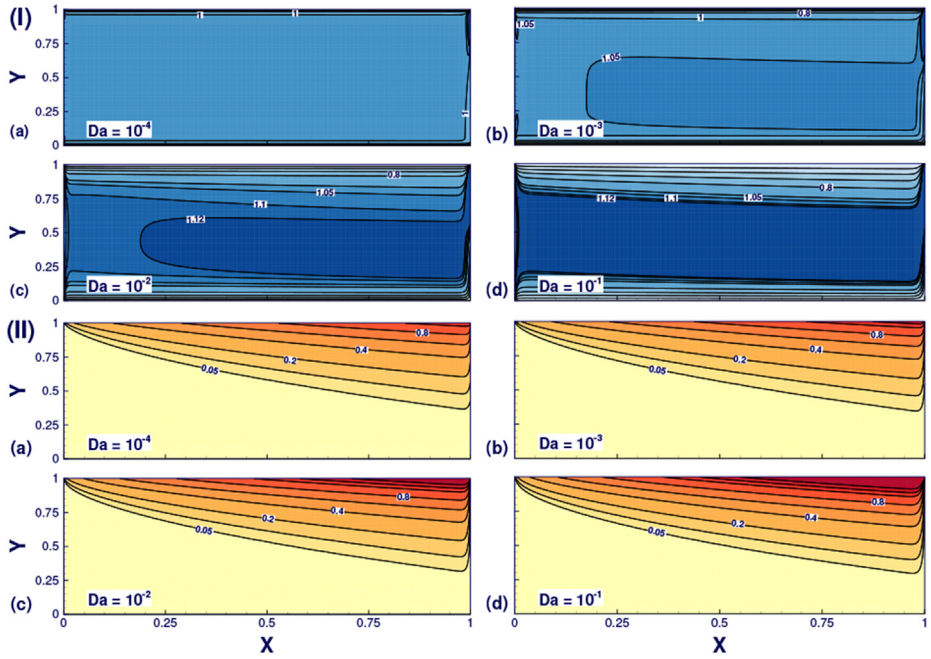

Fig. 7. (I) Velocity and (II) Isotherm contours in FPSC channel for different Darcy number (*Da*) values. The contours are shown at Richardson number, $Ri = 5$, channel inclination angle, $\alpha = 45^{\circ}$ and Radiation parameter, $Rd = 0$.

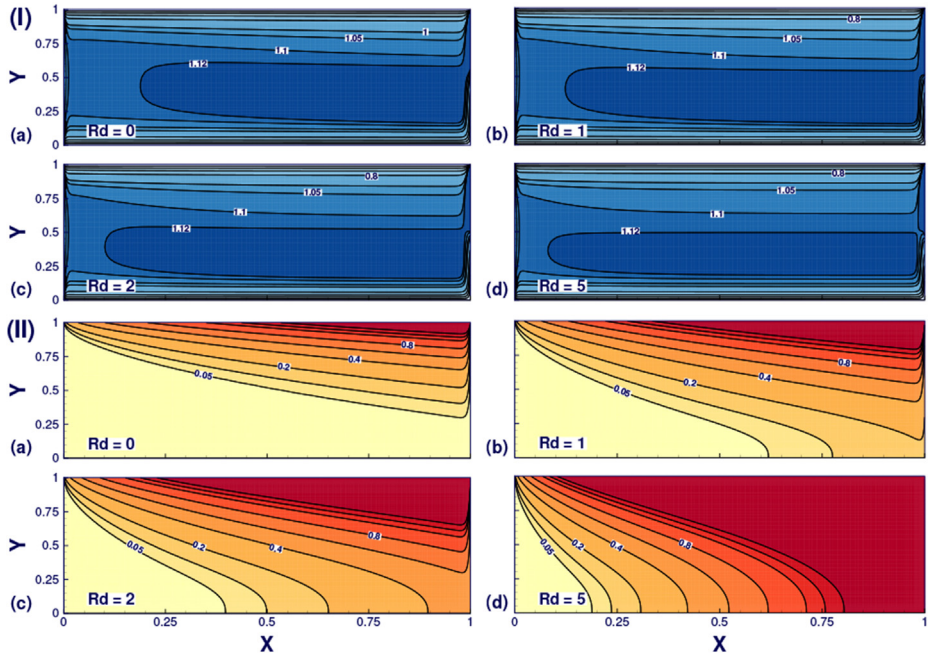

Fig. 8. (I) Velocity and (II) Isotherm contours in FPSC channel for different Radiation parameter (*Rd*) values. The contours are shown at Richardson number, $Ri = 0$, Darcy number, $Da = 10^{-2}$ and channel inclination angle, $\alpha = 45^{\circ}$.

get a fully developed flow at the channel outlet. Hence, velocity distribution only at the outlet is focussed on, and variation in the same concerning the governing parameters of the study is displayed in Fig. 9. It is well-known that the horizontal velocity assumes a parabolic profile in an empty channel under fully developed flow condition. However, in the presence of a porous medium, a flatter velocity profile is witnessed in the centre of the channel, while the thin hydrodynamic boundary layer exists near the channel walls. This occurrence can be ascertained to the fact that the channel is filled with a porous foam, and the resistance curbs the parabolic profile to a flatter curve.

Similar to the above discussion on contours, the influence of each parameter is focussed on to reason and validate earlier mentioned occurrences. Apart from the parameter in focus, $Da = 10^{-2}$, $Ri = 5$, $Rd = 5$, and $\alpha = 45^{\circ}$ are considered for a particular case. At extremities, for a horizontal channel, as seen in velocity contours, instead of simple parabolic shape an inward twist in velocity profile is seen due to the influence of buoyancy. From the

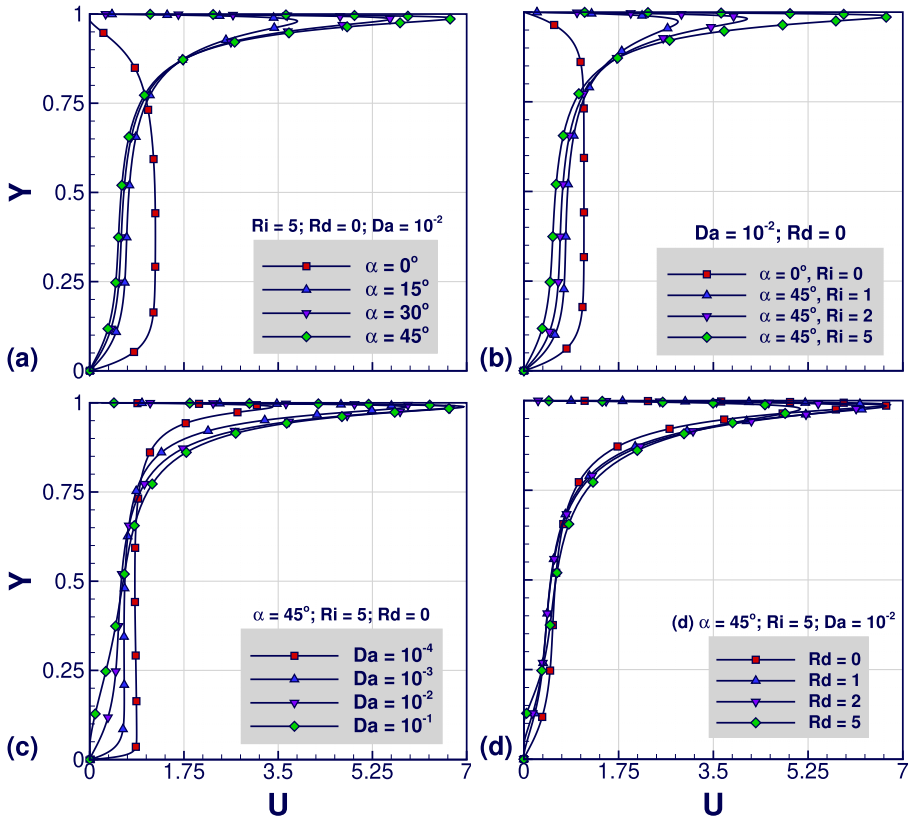

Fig. 9. Non-dimensional x-velocity (U) distribution at the outlet of porous collector channel along vertical direction. The contours are plotted at different values of (a) channel inclination angle (α), (b) Richardson number (Ri), (c) Darcy number (Da), and (d) Radiation parameter (Rd).

variation in flooding of contours at the outlet shown earlier, this can be understood. A sharp increase in flow velocity is witnessed near the absorber wall, which is quite reassuring that the resistance to the flow has been overcome and lesser investment on overcoming the pressure drop across the FPSC channel. At higher inclination angles, thinning of the hydrodynamic boundary layer is evident in Fig. 9(a). The flatter velocity profile discussed before, for a horizontal channel with no consideration of buoyancy, sticks towards absorber wall and a monotonous rise in velocity is lucid (Fig. 9(b)). With reducing resistance to the flow, velocity profile sharply crowds near the absorber wall with rising levels of permeability Fig. 9(c). However, radiation parameter influence, in the presence of buoyancy, is clear with thinning of the hydrodynamic boundary layer at higher Radiation parameter (Fig. 9(d)). Most portion of the outlet fluid tends to attain the velocity value near the absorber wall in comparison with other parameter influences. The maximum velocity value decreases with the increase of Rd value, but the change is meagre.

5.3. Non-dimensional temperature distribution

In general, in a porous medium saturated with a single-phase fluid, the working fluid mixes well. As a result, a flatter velocity profile develops around the centre of the channel, implying the formation of a thin hydrodynamic boundary layer. A significant temperature gradient, therefore, develops in comparison to an empty channel. Variation in thermal gradient at the absorber wall can be further induced through the buoyancy and radiation parameter variation. Non-dimensional temperature distribution at the porous collector channel outlet is detailed in Fig. 10. The non-dimensionalisation of the temperature is performed concerning the absorber plate temperature instead of far-field value and is normalised by the difference of absorber plate temperature and bulk or mean temperature instead of the far-field value. Hence, the values increase from zero starting from the top layer and rise above one, but this temperature indicates the temperature difference between the insulator and the absorber plate. It gives the idea of temperature rise being achieved by the FPSC channel.

For the horizontally aligned channel, the temperature distribution shows a gradual decrease from the absorber wall towards the insulated wall, suggesting a lesser thermal gradient near the absorber wall, as seen through Fig. 10(a) and (b). Overall, by increasing α, Ri and Da, an increasing temperature gradient near the absorber wall is evident. The gradient value decreases during the rise in Radiation parameter, but there is a rise in the temperature difference between the absorber and insulator plates. It should be noted that at $Rd = 5$, for other parameter variation as well, the maximum difference in temperature is the same (around 1.6). Hence, the reader should not be misled that higher Rd provides a higher heat transfer rate for all other parameters being fixed. The temperature gradient decreases, suggesting lower heat dissipation. Further insights on the same can be seen through local Nu pattern.

5.4. Local Nusselt number variation

Post-solving the governing equations numerically, heat transfer at the top-right corner of the outlet of FPSC is quantified through the local Nusselt number, which is shown through Fig. 11(a), (b) and (c) qualitatively. The local Nu is evaluated by the weighting of temperature with velocity field as demonstrated in the literature as [13],

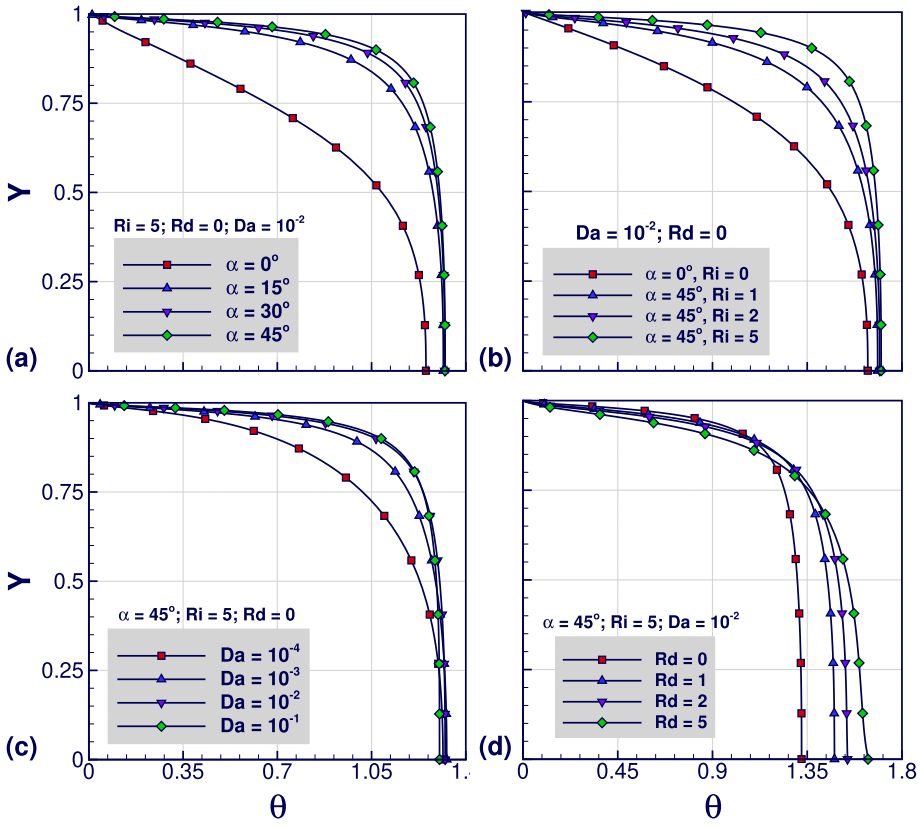

Fig. 10. Non-dimensional temperature (θ) distribution at the outlet of porous collector channel along vertical direction. The contours are plotted at different values of (a) channel inclination angle (α), (b) Richardson number (Ri), (c) Darcy number (Da), and (d) Radiation parameter (Rd).

$$Nu = \frac{D_h}{T_w - T_m(x)} \left(\frac{\partial T}{\partial y}\right)_{y=H}. \tag{7}$$

In the above equation, $T_m(x)$ is the fluid bulk temperature and it is obtained as follows:

$$T_m(x) = \frac{\int_{y=0}^{y=H} uTdy}{\int_{y=0}^{y=H} udy} \tag{8}$$

Impact of the overall variation of velocity and temperature fields on the local Nusselt number is evident. In general, by increasing Rd, due to reducing thermal gradient near absorber plate, Nu value drops. However, exception for this condition exists at $Rd = 5$ for higher values of α, Da and Ri. A steep rise in Nu is reported from $\alpha = 0^\circ$ to $\alpha = 30^\circ$, followed by which the enhancement is meagre. Optimum thermal performance can be expected at an intermediate angle. A monotonic augmentation in Nu is predicated with buoyancy parameter, wherein at $Ri = 5$ maximum value of Nu exists. As Darcy number is increased, more fluid flows through the channel, causing the heat dissipation to rise. Accordingly, the local Nu should increase with Da. However, for a horizontal channel, due to lesser mixing, local Nu decline with Da. The thermal mixing rises when the channel is inclined, causing the local Nu to rise with Da. But again, at higher Rd values, most augmentation is achieved up to $Da = 10^{-2}$ and a slower rise in demonstrated after that.

5.5. Friction factor variation

Although usage of porous media in a channel augments heat dissipation, an unwanted rise in pressure drop occurs. Furthermore, any augmentation in heat transfer through the tuning of parameters like buoyancy or radiation can bring in unwanted pressure variation. Hence, it is utterly important to check for pressure losses to efficiently utilise the available energy with no or a little rise in pumping power. In Fig. 12(a), (b) and (c), the calculated values of non-dimensional pressure drop (friction factor, $f = (H \times \Delta P)/(0.5\rho u^2 L)$) are displayed. In general, by raising Rd, a drop is friction factor values are reported. The intensity of this drop increases with an increase in α and Ri. A possibility for such happenings can be the reduction in viscosity of the fluid at higher Rd values because of the reduction in Pr effect. The easiness of fluid flow through the channel increases with Rd at a higher level of buoyancy parameter. As the channel is inclined clockwise, the flow is assisted by gravity, and hence, general understanding suggests that higher the channel inclination, easier the fluid flow. For a given value of Da, no change occurs in Nu with variation in Rd values. A dominance of permeability nature of the porous medium is suggested over the Radiation parameter. The increment of Darcy number takes the porous channel closer to empty channel-like condition, which supports the decline in pressure drop across channel, rather pumping power.

5.6. Performance Evaluation Criteria (PEC)

After reviewing the increment in heat transfer along with the rise in the friction factor, it becomes vital to analyse the effectiveness of considered parameters to cast a balance between heat transfer augmentation and required efforts of pumping power. Resultingly, a Performance Evaluation Criterion (PEC) has been put forth as [13],

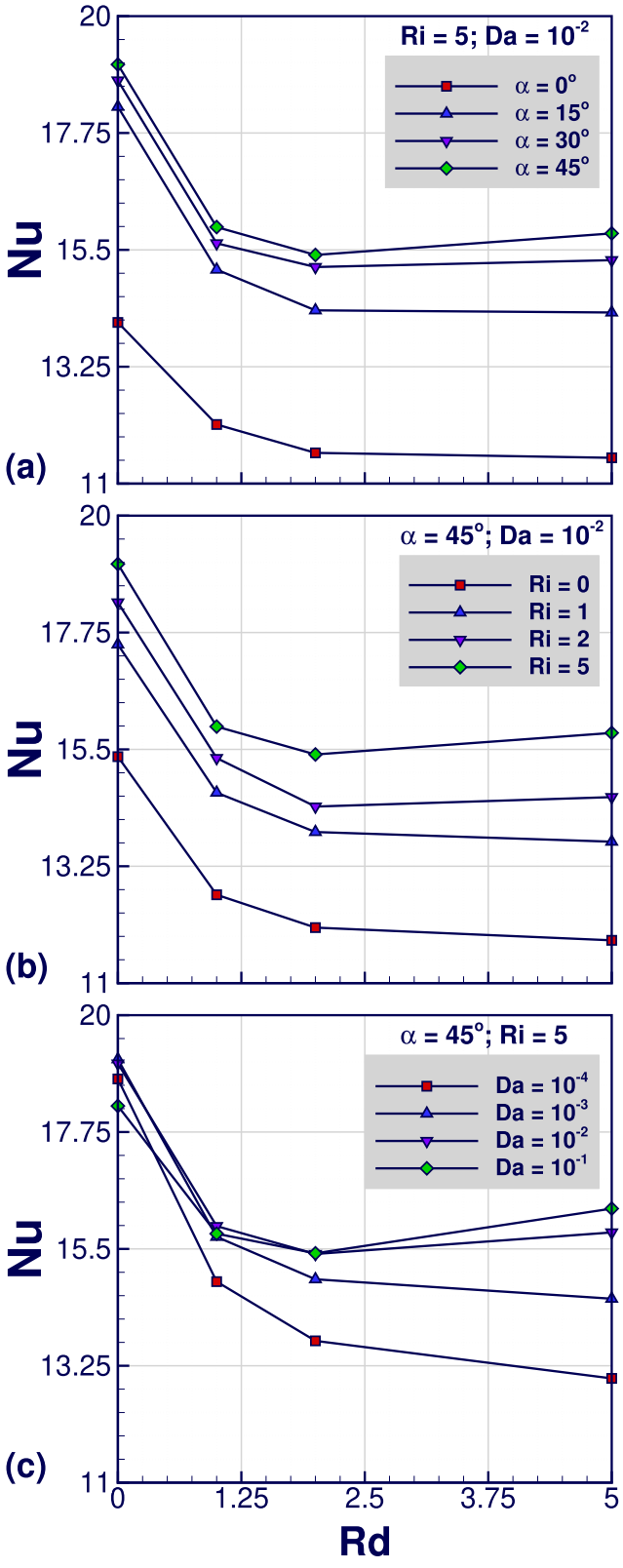

Fig. 11. Local Nusselt number (Nu) variation at the top-right corner of FPSC outlet, plotted at various values of channel inclination angle (α), Richardson number (Ri), Darcy number (Da), and Radiation parameter (Rd).

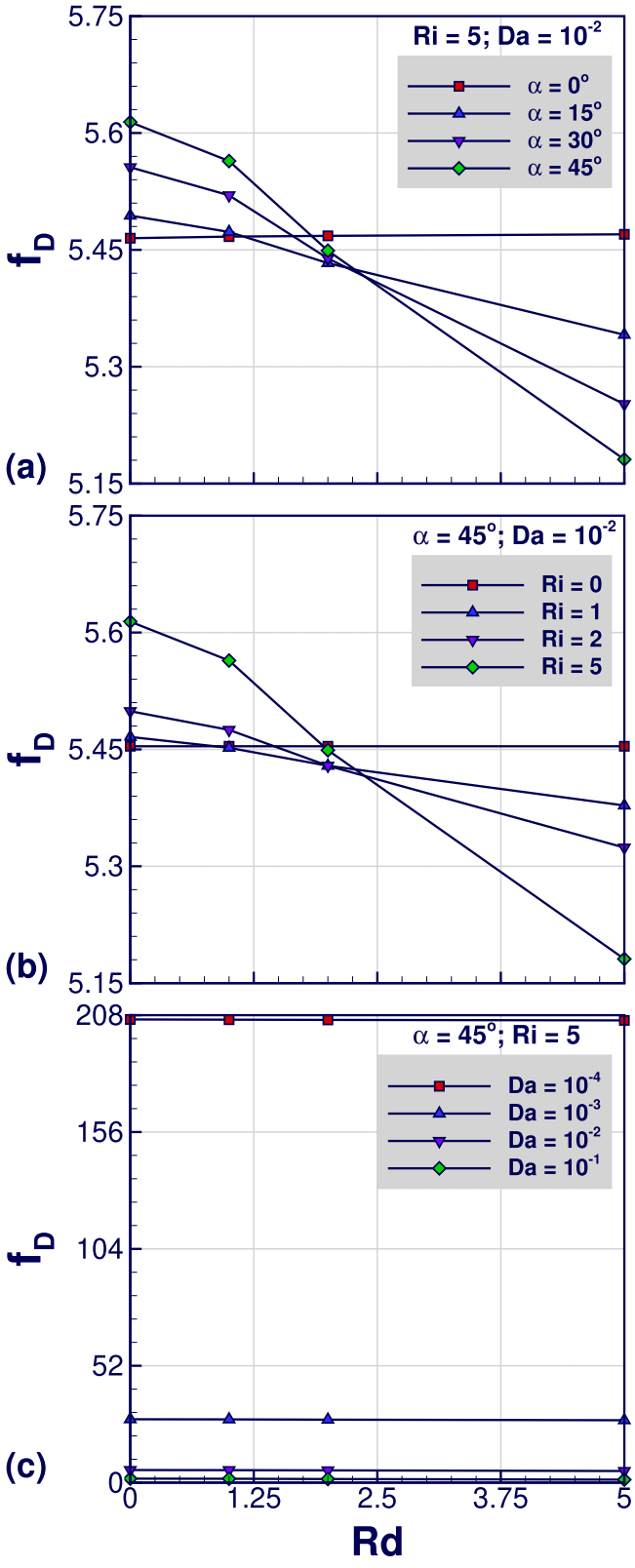

Fig. 12. Friction factor (f_D) variation for FPSC channel, plotted at various values of channel inclination angle (α), Richardson number (Ri), Darcy number (Da), and Radiation parameter (Rd).

$$\mathrm{PEC} = \frac{(Nu_{\alpha}/Nu_{\alpha=0^{o}})}{(f_{D\alpha}/f_{D\alpha=0^{o}})^{1/3}}, \tag{9}$$

wherein Nu_{α} and $f_{D\alpha}$ are local Nusselt number and friction factor at a given channel inclination angle. The subscript '$\alpha = 0^{o}$' suggests a similar meaning for horizontal channel configuration. In the study, performance has been calculated concerning the horizontal configuration for the respective Richardson number, Darcy number and Radiation parameter value. Details of the same are given in Table 2. It is seen that although some configuration at the extreme parameter values offers significant augmentation in heat transfer, the associated pressure drop penalty is quite significant. A maximum value of PEC = 1.628 is reported at $\alpha = 45^{o}$, $Rd = 5$, $Ri = 5$ and $Da = 10^{-1}$. When the PEC values were evaluated with reference to a horizontal empty channel for the respective Ri, a maximum PEC of 1.614 is predicted at the same point. Further, higher PEC values are observed at $\alpha = 15^{o}$, $Rd = 5$, $Ri = 5$ and $Da = 10^{-1}$ and $\alpha = 45^{o}$, $Rd = 5$, $Ri = 5$ and $Da = 10^{-1}$. Better performance can be expected at higher radiation parameter, higher permeability and higher channel inclination to achieve maximum heat transfer through buoyancy effects, with least pumping power loss. Such an occurrence assures a good connection with the practice, as $\alpha = 45^{o}$ is well-known to be desired inclination angle for the collector channel in reality. However, at intermediate angles, most improvement in PEC is reported. At $\alpha = 15^{o}$, in increment of 32.002% is obtained in PEC with respect to $\alpha = 0^{o}$. Further, the increment drops down to 5.299% and 4.596%, between $\alpha = 15^{o}$ and $\alpha = 30^{o}$, and $\alpha = 30^{o}$ and $\alpha = 15^{o}$, respectively. The percentage increment in PEC changes to 20.642%, 6.143% and 4.596% when calculated with respect to the horizontal empty channel for the respective angle ranges. An optimum angle of inclination, therefore, exists between $\alpha = 15^{o}$ and $\alpha = 30^{o}$ wherein maximum increment in PEC can occur, beyond that, the performance improves by increasing channel inclination angle but only nominal (below 5%). When the angle is increased, the ease of fluid flowing increases, but the effective exchange of heat between the absorber plate and working fluid is necessary, and hence, intermediate angles provided a maximum increment in the overall performance.

5.7. Darcy-Brinkman-Forchheimer extended model vs. Darcy-Brinkman model

In the literature, for the given combination of parameters, under the influence of buoyancy and Radiation parameters, the inertial resistance from porous media theory has not been tested for the application. Hence, a comment on the usage of the Forchheimer term is provided along with the combination of Darcy term. Darcy-Brinkman-Forchheimer (D-B-F) and Darcy-Brinkman (D-B) cases are compared for PEC values at various Da, Ri and Rd values for $\alpha = 45^{o}$. The percentage differences are calculated with respect to the D-B-F model, as it is considered to be the more accurate model because it considers both inertial and viscous resistance. The maximum differences in Nu and f_D, calculated concerning D-B-F model are 9.767% and 72.913%, respectively. Perhaps the comparison of PEC values can give an even comparison, which is given in Table 3. The maximum difference now changes to 56.829%, which is still quite significant. Therefore, it is seen that the *inclusion of the Forchheimer term is indeed necessary and that only Darcy-Brinkman model cannot predict the variations in hydrodynamic and thermal fields in the present computational domain accurately.*

6. Conclusions

Performance improvement of an FPSC channel is studied using a numerical approach based on computational fluid dynamics opensource tool OpenFOAM. The channel is filled with porous metal-foam, and its hydrodynamics and thermal performance can be improved for domestic and industrial water heating applications. Darcy-Brinkman-Forchheimer extended model for realising porous medium, along with Rosseland approximation for radiation and Boussinesq approximation for buoyancy inclusion is applied on the generic 'buoyantBoussinesqSimpleFoam' solver of OpenFOAM. Sufficient agreement with experimental results from literature has been shown for the current numerical recipe. Conventional numerical studies on solar collectors often model the channel to be horizontal or without any consideration of buoyancy or channel inclination. The present study takes into account both the factors and tends to determine their effects on the performance of the Flat plate solar collector. The results show that both flow and thermal fields vary significantly for inclined channels with consideration of gravity than the horizontal channel without any. Also, the Rosseland model has been implemented for the considered channel configuration for the first time, and results imply that the implementation of this model predicts lower values of local Nusselt number and friction factor as the radiation insolation parameter, Rd is increased. An overall increment in heat transfer is reported with increasing Darcy number, Da, Richardson number, Ri and channel inclination angle, α. Conversely, friction factor is shown to decrease with Da, Ri, Rd and α. The resulting efficiency of various configurations is evaluated using the Performance Evaluation Criteria (PEC), and details of the optimum parameter ranges are given. An

Table 2
Performance evaluation criteria (PEC) calculated with respect to channel inclination angle, $\alpha = 0^{\circ}$ at respective Richardson number (Ri) at various channel inclination angle, Darcy number (Da), and Radiation parameter (Rd) values.

	Rd	Da											
		$\alpha = 15^{\circ}$				$\alpha = 30^{\circ}$				$\alpha = 45^{\circ}$			
		10^{-4}	10^{-3}	10^{-2}	10^{-1}	10^{-4}	10^{-3}	10^{-2}	10^{-1}	10^{-4}	10^{-3}	10^{-2}	10^{-1}
$Ri = 1$	0	1.010	1.048	1.091	1.161	1.023	1.059	1.132	1.206	1.027	1.089	1.148	1.238
	1	1.010	1.028	1.099	1.170	1.017	1.055	1.144	1.211	1.019	1.082	1.171	1.237
	2	0.990	1.033	1.095	1.164	1.009	1.067	1.140	1.220	1.024	1.078	1.162	1.250
	5	1.010	1.024	1.096	1.166	1.013	1.064	1.159	1.240	1.021	1.068	1.185	1.275
$Ri = 2$	0	1.018	1.081	1.155	1.250	1.032	1.109	1.184	1.288	1.054	1.134	1.215	1.303
	1	1.013	1.068	1.148	1.249	1.032	1.112	1.187	1.274	1.042	1.135	1.220	1.302
	2	1.026	1.063	1.149	1.235	1.033	1.094	1.205	1.282	1.058	1.137	1.210	1.312
	5	1.007	1.073	1.154	1.248	1.016	1.116	1.204	1.332	1.026	1.141	1.258	1.380
$Ri = 5$	0	1.049	1.144	1.292	1.471	1.071	1.187	1.323	1.489	1.098	1.207	1.340	1.472
	1	1.047	1.132	1.245	1.421	1.073	1.181	1.283	1.428	1.114	1.217	1.305	1.440
	2	1.041	1.120	1.239	1.405	1.074	1.172	1.311	1.456	1.099	1.215	1.330	1.454
	5	1.039	1.123	1.253	1.458	1.053	1.193	1.349	1.553	1.087	1.227	1.401	1.628

Table 3
Performance evaluation criteria (PEC) comparison between the extended Darcy-Brinkman-Forchheimer (D-B-F) model with Darcy-Brinkman (D-B) model at various Darcy number (*Da*), and Radiation parameter (*Rd*) values for fixed channel inclination angle, $\alpha = 45^{\circ}$ and Richardson number, $Ri = 5$.

Rd	*Da*											
	D-B-F Model				D-B Model				Percentage Deviation (%)			
	10^{-4}	10^{-3}	10^{-2}	10^{-1}	10^{-4}	10^{-3}	10^{-2}	10^{-1}	10^{-4}	10^{-3}	10^{-2}	10^{-1}
0	1.098	1.207	1.340	1.472	1.017	0.931	0.802	0.699	7.341	22.840	40.154	52.532
1	1.114	1.217	1.305	1.440	1.011	0.947	0.787	0.680	9.182	22.229	39.706	52.775
2	1.099	1.215	1.330	1.454	0.999	0.943	0.795	0.668	9.077	22.394	40.252	54.044
5	1.087	1.227	1.401	1.628	0.999	0.948	0.811	0.703	8.141	22.742	42.084	56.829

increment in performance is assured by the use of porous metal foam for better thermal mixing, along with buoyancy parameter and Radiation parameter. Perhaps medium range angles provide the maximum thermal performance increment, with porous fillings of higher permeability. This information should be helpful for further experimental work on the present case, to check for the clockwise inclination along with porous material and buoyancy parameter influences. A comment on the inclusion of the Forchheimer term in the current flow regime is also given. It is confirmed that using extended Darcy-Brinkman-Forchheimer model for modelling the porous channel would be proper. In future, Response Surface Methodology (RSM) can be applied for studying intricate details on the sensitivity of channel inclination angle and Richardson number.

Acknowledgment

One of the authors, S. Dhinakaran, gratefully acknowledges the fund received from Council of Scientific & Industrial Research (CSIR), Government of India, through a project grant (Project Reference No. 22(0642)/13/EMR-II) for carrying out this work.

References

[1] C.G. Granqvist, Transparent conductors as solar energy materials: a panoramic review, Sol. Energy Mater. Sol. Cells 91 (17) (2007) 1529–1598.
[2] P. Vadász, Emerging Topics in Heat and Mass Transfer in Porous Media: from Bioengineering and Microelectronics to Nanotechnology, vol. 22, Springer Science & Business Media, 2008.
[3] D. Poulikakos, M. Kazmierczak, Forced convection in a duct partially filled with a porous material, J. Heat Transf. 109 (3) (1987) 653–662.
[4] F. Lansing, V. Clarke, R. Reynolds, A high performance porous flat-plate solar collector, Energy 4 (4) (1979) 685–694.
[5] M. Sorour, A new type of solar water heater, Int. J. Energy Res. 9 (1) (1985) 27–32.
[6] C. Kleinstreuer, H. Chiang, Analysis of a porous-medium solar collector, Heat Transf. Eng. 11 (2) (1990) 45–55.
[7] K. Sopian, W.R.W. Daud, M.Y. Othman, B. Yatim, et al., Thermal performance of the double-pass solar collector with and without porous media, Renew. Energy 18 (4) (1999) 557–564.
[8] B. Yousef, N. Adam, Performance analysis for flat plate collector with and without porous media, J. Energy South. Afr. 19 (4) (2008) 32–42.
[9] A.Y. Bashria, N.M. Adam, Performance analysis of single and double passes flat plate collector with and without porous media, J. Mech. Eng. 58 (5–6) (2008) 275–290.
[10] H. Xu, L. Gong, S. Huang, M. Xu, Non-equilibrium heat transfer in metal-foam solar collector with no-slip boundary condition, Int. J. Heat Mass Transf. 76 (2014) 357–365.
[11] H.J. Jouybari, S. Saedodin, A. Zamzamian, M.E. Nimvari, S. Wongwises, Effects of porous material and nanoparticles on the thermal performance of a flat plate solar collector: an experimental study, Renew. Energy 114 (2017) 1407–1418.
[12] H.J. Jouybari, S. Saedodin, A. Zamzamian, M.E. Nimvari, Experimental investigation of thermal performance and entropy generation of a flat-plate solar collector filled with porous media, Appl. Therm. Eng. 127 (2017) 1506–1517.
[13] S. Saedodin, S. Zamzamian, M.E. Nimvari, S. Wongwises, H.J. Jouybari, Performance evaluation of a flat-plate solar collector filled with porous metal foam: experimental and numerical analysis, Energy Convers. Manag. 153 (2017) 278–287.
[14] M. Al-Nimr, M. Alkam, A modified tubeless solar collector partially filled with porous substrate, Renew. Energy 13 (2) (1998) 165–173.
[15] M. Alkam, M. Al-Nimr, Solar collectors with tubes partially filled with porous substrates, J. Sol. Energy Eng. 121 (1) (1999) 20–24.
[16] M. Kareem, K. Habib, S. Sulaiman, Comparative study of single pass collector and double pass solar collector filled with porous media, Asian Journal of Scientific Research 6 (3) (2013) 445–455.
[17] S. Rashidi, M. Bovand, J. Esfahani, Heat transfer enhancement and pressure drop penalty in porous solar heat exchangers: a sensitivity analysis, Energy Convers. Manag. 103 (2015) 726–738.
[18] M. Bovand, S. Rashidi, J. Esfahani, Heat transfer enhancement and pressure drop penalty in porous solar heaters: numerical simulations, Sol. Energy 123 (2016) 145–159.
[19] C.-C. Chen, P.-C. Huang, Numerical study of heat transfer enhancement for a novel flat-plate solar water collector using metal-foam blocks, Int. J. Heat Mass Transf. 55 (23–24) (2012) 6734–6756.
[20] S. Hirasawa, R. Tsubota, T. Kawanami, K. Shirai, Reduction of heat loss from solar thermal collector by diminishing natural convection with high-porosity porous medium, Sol. Energy 97 (2013) 305–313.
[21] P.-C. Huang, C.-C. Chen, H.-Y. Hwang, Thermal enhancement in a flat-plate solar water collector by flow pulsation and metal-foam blocks, Int. J. Heat Mass Transf. 61 (2013) 696–720.
[22] Z. Chen, M. Gu, D. Peng, Heat transfer performance analysis of a solar flat-plate collector with an integrated metal foam porous structure filled with paraffin, Appl. Therm. Eng. 30 (14–15) (2010) 1967–1973.
[23] K. Anirudh, S. Dhinakaran, Performance improvement of a flat-plate solar collector by inserting intermittent porous blocks, Renew. Energy 145 (2020) 428–441.
[24] R. Holdich, Fundamentals of Particle Technology, Midland Information Technology and Publishing, 2002, ISBN 9780954388102.
[25] S. Dhinakaran, J. Ponmozhi, Heat transfer from a permeable square cylinder to a flowing fluid, Energy Convers. Manag. 52 (5) (2011) 2170–2182.
[26] T. Vijaybabu, K. Anirudh, S. Dhinakaran, Mixed convective heat transfer from a permeable square cylinder: a lattice Boltzmann analysis, Int. J. Heat Mass Transf. 115 (2017) 854–870.
[27] T. Vijaybabu, K. Anirudh, S. Dhinakaran, Lattice Boltzmann simulations of flow and heat transfer from a permeable triangular cylinder under the influence of aiding buoyancy, Int. J. Heat Mass Transf. 117 (2018) 799–817.
[28] T. Vijaybabu, K. Anirudh, S. Dhinakaran, LBM simulation of unsteady flow and heat transfer from a diamond-shaped porous cylinder, Int. J. Heat Mass Transf. 120 (2018) 267–283.
[29] K. Anirudh, S. Dhinakaran, On the onset of vortex shedding past a two-dimensional porous square cylinder, J. Wind Eng. Ind. Aerodyn. 179 (2018) 200–214.
[30] C. Sivaraj, M.A. Sheremet, Natural convection coupled with thermal radiation in a square porous cavity having a heated plate inside, Transp. Porous Media 114 (3) (2016) 843–857.
[31] H.G. Weller, G. Tabor, H. Jasak, C. Fureby, A tensorial approach to computational continuum mechanics using object-oriented techniques, Comput. Phys. 12 (6) (1998) 620–631.
[32] F.P. Kärrholm, Numerical Modelling of Diesel Spray Injection, Turbulence Interaction and Combustion, Chalmers University of Technology Gothenburg, 2008.
[33] Y. Varol, H.F. Oztop, A. Koca, F. Ozgen, Natural convection and fluid flow in inclined enclosure with a corner heater, Appl. Therm. Eng. 29 (2–3) (2009) 340–350.
[34] T. Basak, S. Roy, T. Paul, I. Pop, Natural convection in a square cavity filled with a porous medium: effects of various thermal boundary conditions, Int. J. Heat Mass Transf. 49 (7–8) (2006) 1430–1441.
[35] S.E. Ahmed, H.F. Oztop, K. Al-Salem, Natural convection coupled with radiation heat transfer in an inclined porous cavity with corner heater, Computers & Fluids 102 (2014) 74–84.
[36] K. Anirudh, S. Dhinakaran, Effects of Prandtl number on the forced convection heat transfer from a porous square cylinder, Int. J. Heat Mass Transf. 126 (2018) 1358–1375.